ADVANCES IN GEODESY AND GEOINFORMATION
(formerly GEODESY AND CARTOGRAPHY)
Vol. 74, no. 1, article no. e64, 2025

https://doi.org/10.24425/agg.2025.154148

Original paper

Part of Topical collection:
"Advancements in Applied Geoinformatics"

Transforming GRACE mascon TWS-L3 data into vertical displacements using a regression approach: a case study of the Türkiye region

Cüneyt Aydın, Özge Güneş*, Beyza Güney

Yildiz Technical University, Esenler, Türkiye
e-mail: caydin@yildiz.edu.tr; ORCID: http://orcid.org/0000-0003-0888-0316
e-mail: ozgeg@yildiz.edu.tr; ORCID: http://orcid.org/0000-0001-7576-621X
e-mail: beyza.guney@std.yildiz.edu.tr; ORCID: http://orcid.org/0009-0004-2119-1747

*Corresponding author: Özge Güneş, e-mail: ozgeg@yildiz.edu.tr

Received: 2024-10-29 / Accepted: 2025-02-27

Abstract: The Gravity Recovery and Climate Experiment (GRACE) and GRACE Follow-On satellite missions have been monitoring hydrological events on Earth's surface for nearly two decades. Monthly gravity solutions from these satellites are available as Level-2 (L2) spherical harmonic coefficients or as ready-to-use Level-3 (L3) data, typically representing Total Water Storage (TWS) variations. L3 data, such as Goddard Space Flight Center (GSFC) mascon data, include essential corrections like post-glacial rebound and signal-leakage, and precisely represent TWS variations for specific regions, such as river basins, without additional corrections. However, certain geopotential changes, such as groundwater-induced vertical displacements, gravity anomalies and geoid height changes cannot be directly obtained from these data. To evaluate these geopotential changes, L3 data needs to be transformed into harmonic coefficient solutions. While this method is more computationally demanding compared to adapting L2 data with necessary corrections, the question remains: How can L3 TWS data be directly transformed into other potential changes? In this study, we propose a regression approach for the Türkiye region, using approximately hundred GSFC-mascon blocks to convert TWS into groundwater-induced vertical displacements. Transformation parameters are estimated by considering outcomes from L2 data, specifically selecting DDK2-filtered data. The ratio between vertical displacement and TWS for each mascon is modeled by a quadratic function based on TWS magnitudes. Investigating residuals reveals a time-dependent pattern, which requires a second regression to model this aspect. This two-step regression approach successfully transforms TWS into vertical displacements, with a root-mean-square error of about half a millimeter, providing satisfactory results for the region.

Keywords: Türkiye, GRACE, TWS, mascon, groundwater-induced vertical displacements

1. Introduction

The Gravity Recovery and Climate Experiment (GRACE) and its successor, GRACE-Follow On (GRACE-FO) missions, have been monitoring temporal variations in Earth's gravitational field for the past two decades. Both the GRACE and GRACE-FO datasets, collectively referred to as GRACE data, have been extensively utilized to track Total Water Storage (TWS) variations, playing a crucial role in assessing hydrological changes. These monthly solutions are produced in various forms, but the two most widely used formats are Level-2 (L2) spherical harmonic coefficients data and preprocessed Level-3 (L3) data. The L2 data, while flexible and widely used, requires filtering, such as the application of the DDK (decorrelation filter) (Kusche et al., 2009), along with error reduction by users. On the other hand, the L3 data such as mascon solutions are pre-filtered, regularized, and corrected for signal leakage, providing a ready-to-use alternative. Mascon solutions directly represent TWS changes in terms of Equivalent Water Thicknesses (EWT), making them practical for regional analyses, but their preprocessed nature limits direct calculations of potential changes such as vertical displacements.

L2 datasets, despite their complexity, enable transformations into various gravitational changes, including total water storage, geoid height, and vertical displacements. These transformations are crucial for understanding hydrological mass changes, and there is a potential for integration with other remote sensing techniques like the Global Navigation Satellite System (GNSS) and hydrological models. This integration enhances the sensitivity of mass variability assessments and provides more comprehensive insights into regional water dynamics.

Numerous studies have focused on transforming TWS into displacement time series, with most relying on the L2 spherical harmonic coefficient datasets (Tregoning et al., 2009; Tesmer et al., 2011; Fu and Freymueller, 2012; Fu et al., 2012; Liu et al., 2014; Hao et al., 2016; Tan et al., 2016; Yin et al., 2020; Tangdamrongsub and Sprlak, 2021). For example, Tesmer et al. (2011) reported the stability of GRACE monthly L2 gravity products with a precision of 1.2 mm for vertical deformation, using data from three different GRACE data centers. About 80% of surveyed stations showed common signals when compared with GPS data. Liu et al. (2014) also highlighted strong correlations between GRACE-derived vertical displacements and GPS-observed seasonal position variations in the North China Plain. Similar findings were reported by Hao et al. (2016) for the southeastern Tibetan Plateau, underscoring the reliability of L2 data in capturing hydrological effects on vertical displacements.

Although L2 data has been primarily used in such transformations, recent research has explored the potential of L3 mascon solutions. Several studies have successfully transformed mascon data into spherical harmonic coefficients to calculate displacements, yielding promising results in regions like the Yangtze River Basin (Lenczuk et al., 2020; Wang et al., 2020; Wang et al., 2023). For instance, Lenczuk et al. (2020) analyzed hydrology-induced Earth crust deformations across Europe using Center for Space Research (CSR) mascon solutions, estimating vertical displacements for 29 major European river basins. Their findings highlighted that GRACE-derived results provided more precise insights into large-scale hydrological changes compared to two hydrological models: the

WaterGAP Global Hydrological Model (WGHM) and the Global Land Data Assimilation System (GLDAS). Wang et al. (2023) compared vertical displacements derived from both spherical harmonic and mascon products in the Amazon Basin (sources from the CSR, German Research Centre for Geosciences (GFZ), Jet Propulsion Laboratory (JPL), and Goddard Space Flight Center (GSFC)), showing that mascon solutions provided better agreement with GNSS displacement time series than spherical harmonic-derived solutions. Similar conclusions also reached by Wang et al. (2020) for the Yangtze River Basin.

While L2 data allows for greater flexibility in transformation into various potential changes, it requires significant post-processing, which can be computationally intensive. In contrast, L3 mascon solutions, although easier to use, are preprocessed and thus limit direct calculations of some geophysical parameters, such as vertical displacements. This leads to a crucial question: How can L3 TWS time series be directly converted into alternative potential variations? In this study, we address this limitation by developing a method that directly converts ready-to-use TWS-L3 mascon data into vertical displacement time series through a time-dependent regression approach. By using coefficients derived from our regression model, we transform pre-processed mascon data into vertical displacements specifically for the Türkiye region. This approach allows for a more direct and efficient application of L3 mascon data in assessing hydrology-induced displacements. This paper introduces our algorithm and presents initial findings for the Türkiye region.

2. Materials and methods

2.1. GRACE TWS and vertical displacement calculations

The redistribution of mass on Earth's surface, particularly in the form of TWS changes, is driven by hydrological processes such as groundwater depletion, surface water fluctuations, snowmelt, and variations in soil moisture across all vertical layers. Each of these layers responds differently to seasonal and long-term shifts, causing mass changes that can be detected through alterations in Earth's time-variable gravitational field. The movement of water mass within these layers can result in elastic deformation of the Earth's crust, which is supported by the underlying mantle. GRACE-derived datasets enable the computation of these mass-induced geopotential changes, reflected both as TWS anomalies and the corresponding vertical displacements.

These TWS changes observed by GRACE satellites can be computed using spherical harmonics, as described by the following equation (Wahr et al., 1998):

$$\Delta TWS\,(\theta,\lambda) = a\frac{\rho_{\text{ave}}}{3\rho_w}\sum_{n=1}^{n_{\max}}\sum_{m=0}^{n}\overline{P}_{nm}(\cos\theta) + \left(\Delta\overline{C}_{nm}\cos\left(m\lambda\right)\Delta\overline{S}_{nm}\sin\left(m\lambda\right)\right)\frac{2n+1}{1+k_n}. \tag{1}$$

In this equation, (θ, λ) represent colatitude and longitude, respectively, while a denotes the Earth's radius. Constants ρ_{ave} and ρ_w represent the mean Earth's density and water

density, respectively. $\overline{P}_{nm}$ are fully normalized associated Legendre functions for degrees (n) and orders (m), while $\Delta\overline{C}_{nm}$ and $\Delta\overline{S}_{nm}$ are harmonic coefficients of the time-variable Earth's gravity field relative to the average gravity field model. Finally, k_n is the load Love number of degree n (Wahr et al., 1998; Wahr, 2007).

To further extend the hydrological analysis, vertical displacements (Δr) due to changes in mass can also be computed using spherical harmonics, expressed as (van Dam et al., 2007):

$$\Delta r\,(\theta,\lambda) = a\sum_{n=1}^{n_{\max}}\sum_{m=0}^{n}\overline{P}_{nm}(\cos\theta)\left(\Delta\overline{C}_{nm}\cos(m\lambda)+\Delta\overline{S}_{nm}\sin(m\lambda)\right)\frac{h_n}{1+k_n}. \tag{2}$$

Here, h_n is the load Love number of degree n provided by Farrell (1972) in addition to k_n. While these formulas provide a robust method for calculating TWS and vertical displacements using GRACE spherical harmonics (L2), they are not directly applicable to mascon (L3) data. To compute vertical displacements using mascon solutions, mascon mass change is converted into Stokes coefficients ΔC_{nm} and ΔS_{nm} up to desired degree and order by calculating the spherical integrals as given in the following equations (Wahr et al., 1998):

$$\begin{aligned}
\Delta\hat{C}_{nm} &= \frac{1}{a\rho_w}\frac{1}{4\pi}\iint\Delta TWS\,(\theta,\lambda)\,\overline{P}_{nm}(\cos\theta)\cos(m\lambda)\,\mathrm{d}\sigma,\\
\Delta\hat{S}_{nm} &= \frac{1}{a\rho_w}\frac{1}{4\pi}\iint\Delta TWS\,(\theta,\lambda)\,\overline{P}_{nm}(\cos\theta)\sin(m\lambda)\,\mathrm{d}\sigma,\\
\begin{Bmatrix}\Delta C_{nm}\\ \Delta S_{nm}\end{Bmatrix} &= \frac{3\rho_w}{\rho_{\mathrm{ave}}}\frac{1+k_n}{2n+1}\begin{Bmatrix}\Delta\hat{C}_{nm}\\ \Delta\hat{S}_{nm}\end{Bmatrix}.
\end{aligned} \tag{3}$$

These processes require a significant amount of computational effort, and the various corrections applied to calculate the mascon mass change should be restored or repeated as needed before being converted into spherical harmonics. However, not all L3 mascon datasets provide these necessary corrections. Some mascon solutions are directly computed using L1-B data, without offering the required adjustments. On the other hand, we have noticed that a relationship exists between TWS and vertical displacement time-series obtained using Eq. 1 and Eq. 2. This relationship led us to generate a regression model to retrieve the vertical displacements from TWS anomalies for a given computation point. As detailed in the next section, such a model can be produced from a filtered L2 data such as using DDK1, 2, and so on, which has a compatible resolution with the mascon solution in terms of TWS anomalies.

2.2. Data sources and processing

For the computations, we use the CSR Release 06 DDK2 filtered spherical harmonic coefficients up to degree and order 60. These coefficients are provided by CSR through ICGEM web services (https://icgem.gfz-potsdam.de/sl/temporal). The dataset covers the period from April 2002 to December 2022. In this study, the C_{20} harmonic coefficients

are replaced with Satellite Laser Ranging (SLR) observations to enhance accuracy, as suggested by previous studies (Cheng and Ries, 2017; Loomis et al., 2019a; Loomis et al., 2020). We selected the DDK2 filter because the 1 arc degree GSFC mascon solutions represent approximately a 300 km Gaussian filter (Loomis et al. 2019b), while the DDK2 filter corresponds to a spatial filter with a smoothing radius of approximately 340 km (Flechtner et al., 2014). Both filters, while different in their implementation, have similar trends in time series analysis.

GSFC monthly time series of TWS anomalies, presented in the form of mascon solutions of the RL06v02 version, are also used. These solutions are directly derived from the GRACE Level-1B data. The GSFC mascon solutions are derived by removing the GGM05C background static field (Ries et al., 2016) and replacing the C_{20} and C_{30} coefficients as outlined in Technical Note 14 (Sun et al., 2016; Loomis et al., 2020). Additionally, atmosphere and ocean de-aliasing effects are reduced with the method of Dobslaw et al. (2017). The Glacial Isostatic Adjustment (GIA) effect is corrected using the ICE-6G_D model (Peltier et al., 2015), while leakage uncertainties are addressed as provided in Loomis et al. (2020). Consequently, the final TWS anomalies are released as TWS time series after removing the mean over the 2004–2010 time span.

For our analysis, we calculate TWS and vertical displacements using spherical harmonic coefficients filtered with DDK2 based on Eq. 1 and Eq. 2, according to the coordinates with the mascon center points. Furthermore, time differencing is applied to the DDK2 solutions for the 2004–2010 period to ensure consistency.

3. Regression analysis of the functional model between TWS and vertical displacement

As stated in the previous section, TWS and vertical displacement solutions have been computed using spherical harmonic coefficients filtered with DDK2 generated by CSR, according to the Eq. 1 and Eq. 2. To achieve this, we utilized approximately one hundred grid points, each representing the center coordinates of GSFC mascon blocks located on land within the Türkiye region, as shown in Figure 1, to convert TWS data into vertical displacements.

To demonstrate the results of TWS and vertical displacements derived from DDK2-filtered spherical harmonics, Figure 2 presents randomly selected time series from various locations within the study region. In this figure, the blue line represents the TWS time series calculated using Eq. 1, while the orange line depicts the vertical displacement computed based on Eq. 2. Notably, the two time series exhibit inverse movements, indicating that as TWS increases, vertical displacements tend to decrease, and vice versa; this relationship is further emphasized by the fact that TWS is in centimeters of water equivalent (cm EWT), while vertical displacements are expressed in millimeters (mm). This behavior underscores the relationship between water redistribution and surface deformation, showcasing the effective use of L2 data to generate valuable insights into hydrological changes and their impacts on the Earth's surface.

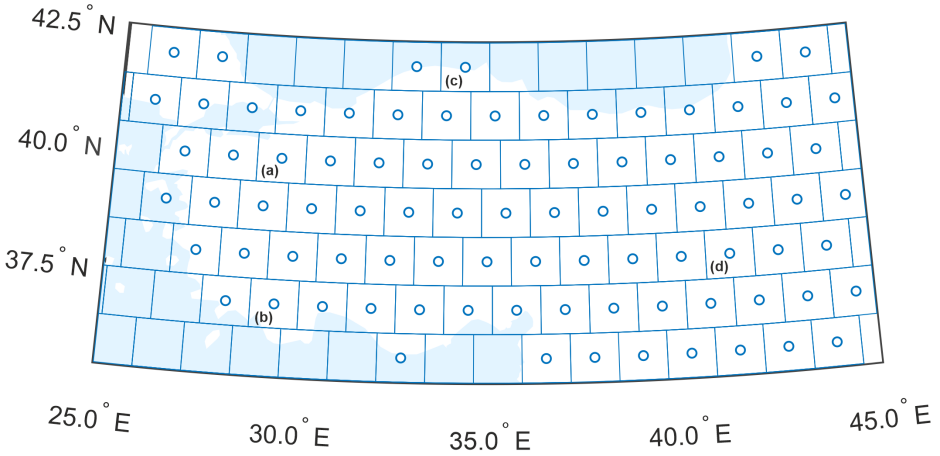

Fig. 1. Mascon blocks in the Türkiye region, with dots representing the center of each mascon block used in this study for calculating TWS and vertical displacements from the CSR DDK2 solutions. The dots labeled from a to d indicate the locations of the time series shown in Figures 2a-d

The trend of mass change in these time series can be determined using the following harmonic regression model:

$$y(t) - e(t) = b_0 + b_1 t + \sum_{i=1}^{2} \left(c_i \cos(\omega_i t) + s_i \sin(\omega_i t)\right). \tag{4}$$

Here, $e(t)$ represents the error term; b_0 is the intercept; b_1 is the linear trend (rate of change); ω_1 and ω_2 are the angular frequencies of the annual and semi-annual periodic signals, respectively; and c and s are the amplitudes of the cosine and sine components. The angular frequencies are typically defined as $\omega_1 = 2\pi/T_1$ (T_1 = 1 year) and $\omega_2 = 2\pi/T_2$ (T_2 = 1/2 year); the amplitude of the signal is defined as $A = \sqrt{c^2 + s^2}$.

For example, at the location indicated in Figure 2a (Lat: 40.00° N, Lon: 29.45° E), which corresponds to one of the time series in the Sakarya Basin in northwestern Türkiye, the trend of mass change is determined based on the harmonic regression model. This analysis reveals a change of -0.17 cm/year in mass, leading to an inverse relationship with vertical displacement, which is found to be 0.25 mm/year. To further explore the relationship between TWS and vertical displacement time series, we calculated the Pearson correlation coefficient of –0.92. This significant correlation suggests that as TWS decreases, vertical displacement tends to increase.

Similarly, Figures 2b, 2c, and 2d present time series from locations corresponding to the Mediterranean, Western Black Sea, and Tigris-Euphrates basins, respectively. Upon examining these regions, it is clear that the TWS and vertical displacement trends exhibit inverse behavior. For instance, in Figure 2d, the magnitude of TWS significantly affects the trend, resulting in a change of –0.84 cm/year. Correspondingly, the vertical displacement time series shows a change of 0.55 mm/year. When comparing Pearson correlation

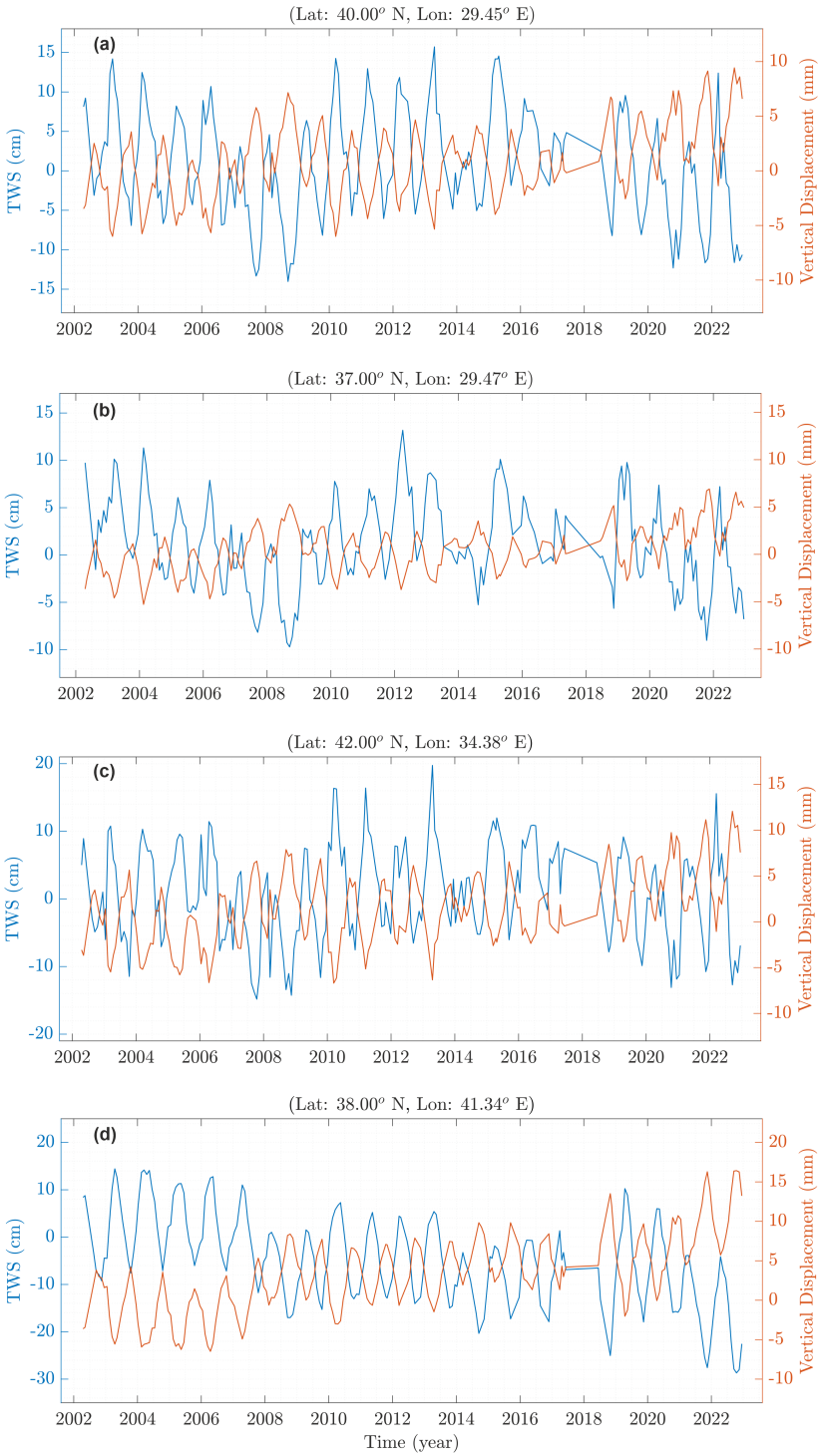

Fig. 2. Example time series of randomly selected DDK2 filtered TWS (blue line) and vertical displacements (orange line) in the Türkiye region

values for these time series in Figures 2b, 2c, and 2d are obtained –0.87, –0.85, and –0.97, respectively. The slightly lower correlation values in Figure 2b (Mediterranean) and Figure 2c (Western Black Sea) suggest that these areas may be influenced by signal leakage and the impact of different layers within the TWS, not solely by groundwater-induced vertical displacements. Subsequently, we computed the mean trend (velocity) for all grids used in this study to provide an overall snapshot. The trend values were determined to be –0.6 mm/year for vertical displacements and 0.4 cm/year for TWS changes. The correlation value across all selected grids in Türkiye was found to be –0.93, reflecting a strong inverse relationship between TWS changes and vertical displacements.

After examining TWS and vertical displacements using the L2 dataset, the analysis focusing on the core objective of this study – the functional relationship between TWS and vertical displacements – has been initiated. This relationship between EWT changes at specific points and vertical displacements is established through regression analysis. The analysis begins with quadratic regression, followed by temporal regression. The quadratic regression, referred to as the first regression in this paper, is a type of second-degree polynomial regression used to model the relationship between a dependent variable (v) and an independent variable (u). This approach is employed when linear regression does not sufficiently explain the data, enabling a more accurate capture of underlying trends. The quadratic regression equation can be expressed as follows:

$$v = a_0 + a_1 u + a_2 u^2. \tag{5}$$

Here, a is the regression coefficients. Temporal regression is designed to model both seasonal (periodic) components and nonlinear trends. This model combines second-degree polynomials with trigonometric components to capture seasonal variations and long-term trends in the time series. The temporal regression model can be formulated as follows:

$$v\,(t) = a_3 + a_4 t + a_5 t^2 + a_6 \sin(wt) + a_7 \cos(wt)\,. \tag{6}$$

In this context, "w" represents the frequency of the seasonal component, expressed as $(2\pi/T)$, where T is the seasonal cycle duration. The regression model in Eq. 6 can be adapted for various seasonal cycle durations. Upon examining the results of the harmonic regression, it has been observed that there is a clear inverse relationship between vertical displacements and TWS as shown in Figure 2. However, it is not possible to derive a common relationship for the points by solely performing linear regression. For this reason, quadratic regression given in Eq. 5 has been attempted to the dataset used in this study. When the regression results were analyzed, a temporal correlation was observed between the two geopotential changes, leading to the application of temporal regression and adapted the Eq. 6 to consider time-dependent regression analysis. The extended formula, as given in Eq. 7, is derived from the results of both regressions to compute vertical displacements (Δr^m) directly from the TWS time series as a final regression model:

$$\begin{aligned}\text{vertical displacement } (\Delta r^m) = {} & (a_0 + a_1 TWS + a_2 TWS^2)\,(10 + TWS) - 100 \\ & - (a_3 + a_4 \Delta t + a_5 \Delta t^2 + a_6 \cos(2\pi\Delta t) + a_7 \sin(2\pi\Delta t) \\ & + a_8 \cos(2\pi\Delta t/15) + a_9 \sin(2\pi\Delta t/15)).\end{aligned} \tag{7}$$

In this functional model, TWS is expressed in decimeters (dm), while vertical displacement (Δr^m) is measured in millimeters (mm). The reference time is set to 2002.2931, which corresponds to the first decimal year date of the GRACE observations. Δt represents the time difference between the reference time and the observation time. As a result, we derive unique 10-parameter transformation equations (referred to as the final regression model), as shown in Eq. 7, and determine the regression coefficients for each grid point to transform TWS into vertical displacements.

When the development of this algorithm is studied using the time series shown in Figure 2, the correlation between the ratio and TWS, as illustrated in Figure 3, becomes evident. It is clear that the linear regression presented in Figures 3a, 3c, 3e and 3g exhibits an inverse relationship. However, a common correlation cannot be established for the points by performing only linear regression. Therefore, Figures 3b, 3d, 3f and 3h demonstrate that the functional relationship shows nonlinearity and varies with the magnitude of the TWS. The ratio corresponds to the division of the scaled displacement in mm by the water height in dm (ratio = (100 + vertical disp. (mm)) / (10 + TWS (dm))). This is why the quadratic model, referred to as the first regression model, is more suitable than the linear one.

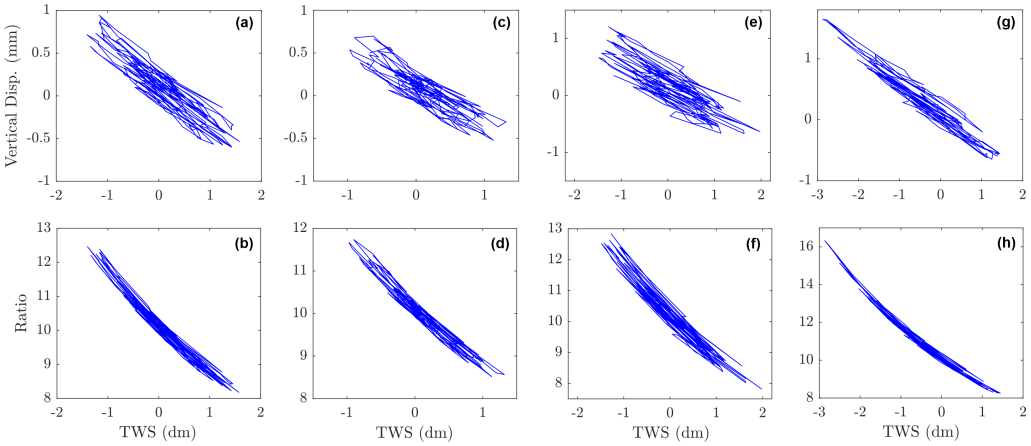

Fig. 3. Functional relationship between vertical displacement-TWS (a, c, e, g) and ratio-TWS (b, d, f, h) for the selected time series. The columns, from left to right, correspond to the time series shown in Figures 2a-d, respectively

The results of the first regression model and the corresponding residuals are presented in Figure 4 for the time series shown in Figure 2a (Lat: 40.00° N and Lon: 29.45° E). For example, after the first regression, the coefficients a expressed in Eq. 5 for this time series are obtained as follows: $a_0 = 10.1076$; $a_1 = -1.4928$ and $a_2 = 0.1804$. The coefficients for the four different time series given in Figure 2 are presented in Table 1.

When reviewing the results of the first regression, it is observed that there are inconsistencies between the modeled vertical displacement and the known values

(Fig. 4a), with irregular patterns still evident in the residuals obtained from the model (Fig. 4b). This situation suggests that previously unconsidered temporal effects may also be present. Consequently, a 10-parameter model has been developed that incorporates time-dependent coefficients.

Table 1. First (quadratic) and final (time-dependent) regression model coefficients for the selected time series

Selected time-series location		Lat: 40.00° N Lon: 29.45° E	Lat: 37.00° N Lon: 29.47° E	Lat: 42.00° N Lon: 34.38° E	Lat: 38.00° N Lon: 41.34° E
Quadratic regression model coefficients	a_0	10.1076	10.0974	10.1689	10.0427
	a_1	–1.4928	–1.4875	–1.5071	–1.5155
	a_2	0.1804	0.1950	0.1680	0.2135
Time-dependent regression model coefficients	a_3	0.5014	0.2291	1.1597	0.5347
	a_4	0.1108	0.1510	0.1306	0.0865
	a_5	–0.0133	–0.0142	–0.0200	–0.0105
	a_6	0.3002	0.0395	0.5217	0.3918
	a_7	0.0130	0.1928	0.5672	–0.5680
	a_8	–0.1309	–0.2132	–0.2854	–0.1149
	a_9	–0.8234	–0.7874	–1.0087	–0.1982

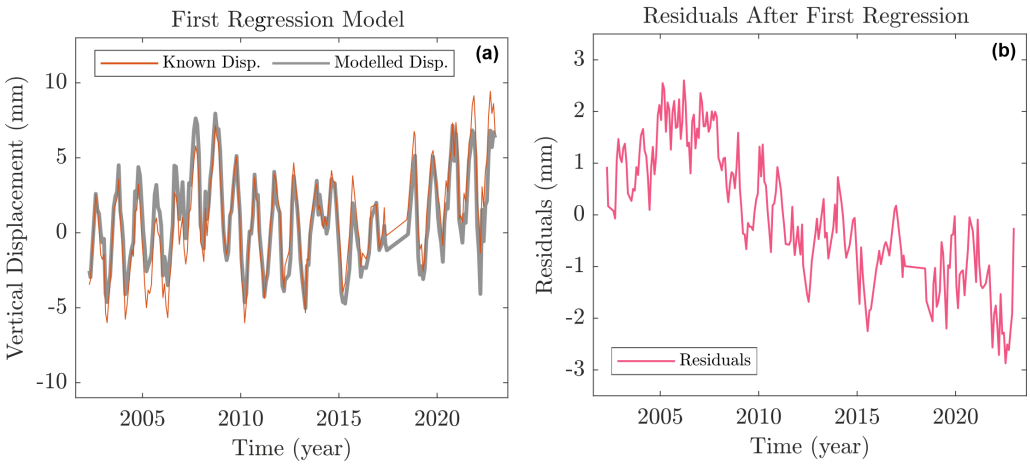

Fig. 4. First regression model results for the given time series in Figure 2a (Lat: 40.00° N, Lon: 29.45° E)

When the final regression is applied, the time-dependent regression coefficients in Eq. 7 for the time series shown in Figure 2 are provided in Table 1. As an example, for the

time series in Figure 2a, the coefficients are obtained as follows: $a_3 = 0.5014$; $a_4 = 0.1108$; $a_5 = -0.0133$; $a_6 = 0.3002$; $a_7 = 0.0130$; $a_8 = -0.1309$ and $a_9 = -0.8234$. Figure 5 also presents the graphs of the final regression model for this time series. These results indicate that, although the values of the time-dependent coefficients are not particularly large, they still influence the residuals. Notably, in Figure 5b, it can be observed that the time-dependent variation in the residuals has decreased and exhibits a pattern similar to that of a normal distribution. This means that the unmodeled parts in quadratic regression model residuals shown in the Figure 4b effectively captured by the time-dependent regression model. Such an outcome highlights the nonlinear and time-dependent relationship between TWS and vertical displacements, making it a significant finding.

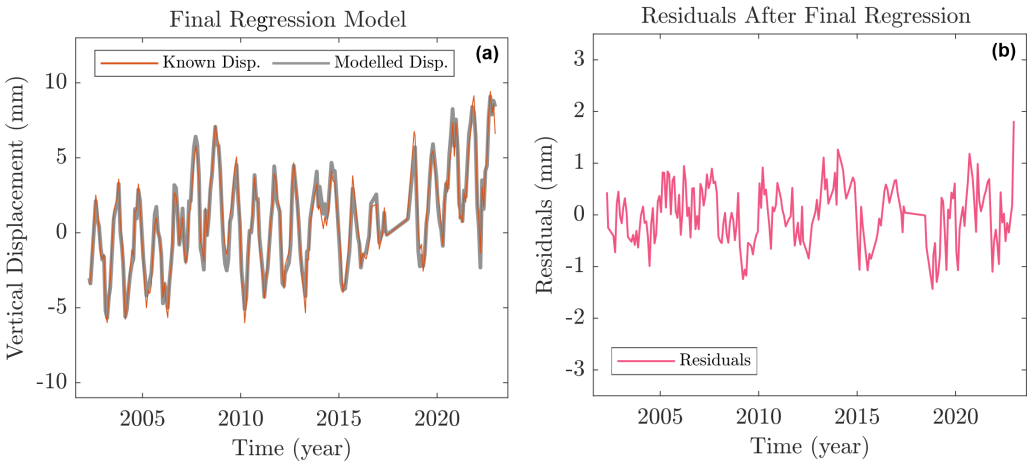

Fig. 5. Final regression model results for the given time series in Figure 2a (Lat: 40.00° N, Lon: 29.45° E)

This improvement is also reflected in the root mean square (RMS) error of the residuals, which are found to be 1.27 mm for the first model and 0.56 mm for the final model. The decrease in the RMS values, in particular, supports the idea that the time-dependent final regression model provides a better explanation of the overall functional relationship.

To compare the results of the first (quadratic) and final (time-dependent) regression models, we also calculated the RMS error for the whole series. After applying the time-dependent regression model, the RMS values were approximately half a millimeter, indicating a high level of accuracy in transforming TWS data into displacement data for the region. The average RMS errors for the time series in the Türkiye region, which comprise nearly one hundred time series, were 1.38 mm for the first regression model and decreased to 0.70 mm for the final regression model. Figure 6 presents the RMS values of the residuals for all-time series.

After assessing the results, we identified that the final regression model is better suited for the functional relationship between TWS and vertical displacement data. We then

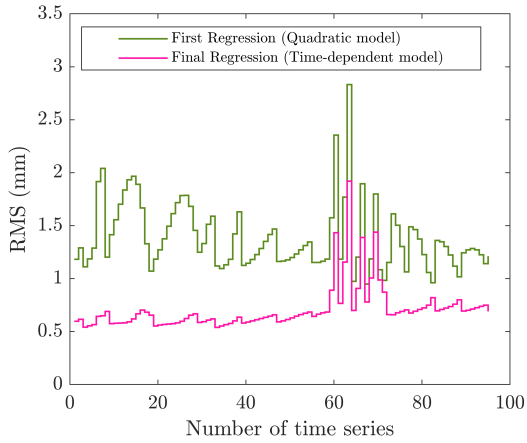

Fig. 6. The RMS errors of the residuals obtained from the first and final regression models. The green line represents the first regression, while the pink line indicates the final regression model

estimated the transformation parameters, allowing us to directly convert the TWS time series into vertical displacements. For internal validation, we utilized the GSFC mascon TWS-L3 time series and transformed it into vertical displacement using the estimated 10-parameter model coefficients.

As an example, Figure 7 presents the GSFC mascon TWS time series, and their corresponding vertical displacements derived from the coefficients listed in Table 1. These time series correspond to the same time series as shown in Figure 2. When comparing Pearson correlation values for these time series, the correlations for Figures 7a, 7b, and 7d exceed –0.93, while Figure 7c shows a correlation of -0.83, similar to the results from the DDK2-TWS time series. This indicates that the final model performs adequately. Overall, the strong inverse correlation across all-time series reinforces the reliability of the model in capturing the relationship between TWS and vertical displacements.

Although the behaviors and patterns of the TWS time series are generally similar across the CSR DDK (L2) and GSFC mascon (L3) datasets, the magnitudes do not consistently match. To further investigate the relationship between vertical displacements derived from these different levels of TWS time series, the Pearson correlation coefficient was analyzed. The correlation between the displacements obtained from the CSR DDK2 TWS and GSFC mascon TWS time series was found to be 0.95 for all-time series included in this study, underscoring the reliability of the transformation process across varied datasets. The developed 10-parameter time-dependent final regression model offers a valuable framework for understanding the relationship between TWS and vertical displacements, facilitating accurate conversions that can be beneficial across various applications within the Türkiye region. These results suggest the model's potential to enhance our understanding of groundwater-induced vertical displacements and associated processes.

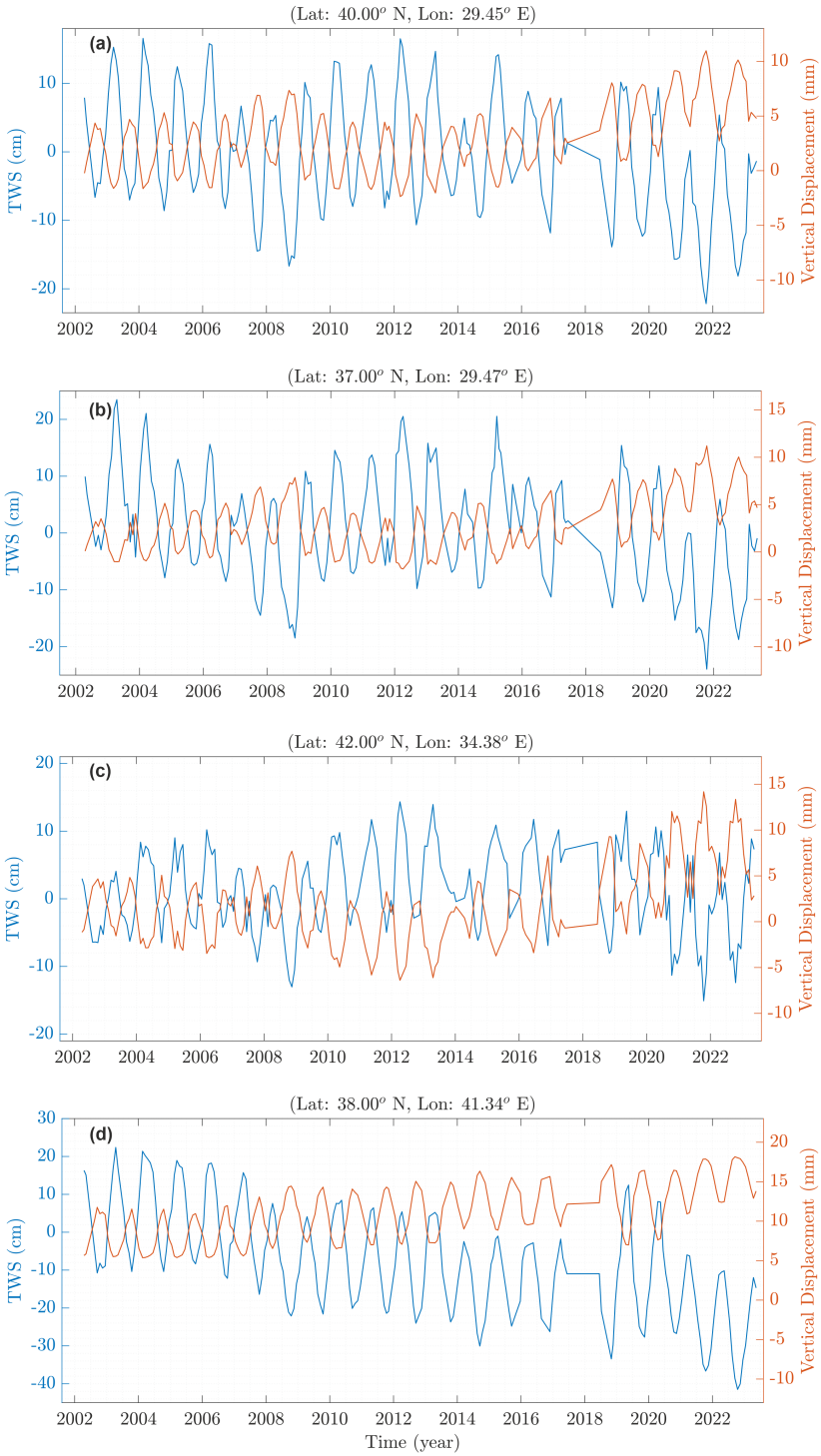

Fig. 7. Time series of example GSFC mascon-based TWS (blue line) and the corresponding vertical displacements (orange line) derived using the final regression model in the Türkiye region

4. Conclusions

In this study, we examined the functional relationship between TWS values and vertical displacements induced by hydrological processes in the Earth's surface, which can be effectively monitored using GRACE and GRACE-FO satellites. These satellites have facilitated global observations of the Earth gravitational field since 2002 exhibiting a high sensitivity to hydrological changes. This sensitivity allows for precise quantification of water variations across continents, enabling researchers to understand better the dynamics of Earth's water systems and their impact on the environment.

Initially, we analyzed the CSR DDK2 (up to 60 degree) data alongside TWS and vertical displacements at the mascon center points for approximately one hundred locations in the Türkiye region. The analysis revealed that the generated TWS and vertical displacement time series exhibit an average correlation exceeding 90% for the study area. This high correlation underscores the potential of TWS as a significant predictor for vertical displacements, highlighting the intricate link between hydrological processes and surface deformation.

To establish a functional relationship between TWS and vertical displacement, a variety of regression methodologies were employed, commencing with linear regression. This initial analysis revealed an inverse correlation between vertical displacements and TWS. However, a definitive relationship could not be established through linear regression alone, prompting an exploration of quadratic regression. This shift in methodology reflects the complexity of the relationship and the need for more sophisticated analytical tools. Following the application of quadratic regression, time-dependent seasonal effects were identified in the residuals, leading to a subsequent regression analysis that produced a ten-parameter functional model linking TWS and vertical displacements. The root mean square (RMS) error, after integrating these time-dependent parameters, is approximately half a millimeter, which is deemed sufficiently accurate for transforming TWS-L3 data into displacements within the analyzed region.

Consequently, we successfully transformed L3 datasets, such as mascon solutions, utilizing these time-dependent regression parameters, which exhibited strong correlations based on internal validations. Thus, the readily available L3 TWS dataset can now be directly transformed into vertical displacements for the corresponding coordinates using the time-dependent parameters obtained from the regression analysis, which are also related to the magnitude of TWS. While the findings provide valuable insights for this study region, it is also essential to highlight several limitations that could influence the accuracy of the results. One such limitation is the potential signal leakage in the GRACE and GRACE-FO data, particularly in regions with heterogeneous hydrological conditions, which may lead to discrepancies in the TWS magnitudes between L2 and L3 data. Although most mascon solutions are corrected for signal leakage, this is not a significant issue for the Türkiye region, except possibly along the Black Sea coast; however, it should be considered for other study regions. Additionally, the preprocessing steps applied to the spherical harmonic coefficients, including filtering and noise reduction techniques, could impact the precision of the model. Furthermore, the resolution of the data plays a crucial role in determining the accuracy of the regression model; finer resolutions may provide

more detailed insights but could also increase computational demands and sensitivity to noise ratio. These factors should be considered in future analyses to refine the model's applicability and interpretability across different regions.

While the limitations discussed above should be considered in refining the model and ensuring its accuracy, the methodologies discussed herein can serve as a foundation for future research and can also support the derivation of other geopotential variations (e.g. geoid change) for ready-to-use time series. By presenting a method for converting L3 TWS data into vertical displacements, we aim to contribute to the ongoing exploration in hydrogeodesy. Future research will focus on conducting external validations using GNSS-derived displacements and refining the regression approach to ensure broader applicability across various regions.

Author contributions

Conceptualization: C.A.; calculation: C.A., O.G., and B.G.; manuscript preparation: C.A. and O.G.; revision: C.A., O.G., and B.G.

Data availability statement

NASA/GSFC mascon solutions are accessible at https://earth.gsfc.nasa.gov/geo/data/grace-mascons, while spherical harmonics are provided by CSR through ICGEM web services at https://icgem.gfz-potsdam.de/sl/temporal. The SLR C20 coefficients have been downloaded from https://download.csr.utexas.edu/pub/slr/degree_2/. The regression coefficients generated in this study are available at the following repository: https://github.com/ozgegunesytu/Regression-Coefficients.

Acknowledgements

The authors would like to express their gratitude to ICGEM and CSR for providing the spherical harmonics and SLR C20 coefficients, as well as to NASA/GSFC for supplying the GRACE mascon solutions. The authors are also thankful to Yildiz Technical University rectorate for providing the MATLAB Academic Full Version.

References

Cheng, M., and Ries, J. (2017). The unexpected signal in GRACE estimates of C20. *J. Geod.*, 91(8), 897–914. DOI: 10.1007/s00190-016-0995-5.

Dobslaw, H., Bergmann-Wolf, I., Dill, R. et al. (2017). Product Description Document for AOD1B Release 06, GRACE 327-750, GFZ German Research Centre for Geosciences, Department 1: Geodesy and Remote Sensing.

Farrell, W.E. (1972). Deformation of the Earth by surface loads. *Rev. Geophys.*, 10(3), 761–797. DOI: 10.1029/RG010i003p00761.

Flechtner, F., Sneeuw, N., and Schuh, W.D. (2014). *Observation of the system earth from space: CHAMP, GRACE, GOCE and future missions*. Berlin, Germany: Springer.

Fu, Y., and Freymueller, J.T. (2012). Seasonal and long-term vertical deformation in the Nepal Himalaya constrained by GPS and GRACE measurements. *J. Geophys. Res. Solid Earth*, 117(B3). DOI: 10.1029/2011JB008925.

Fu, Y., Freymueller, J.T., and Jensen, T. (2012). Seasonal hydrological loading in southern Alaska observed by GPS and GRACE. *Geophys. Res. Lett.*, 39, L15310. DOI: 10.1029/2012GL052453.

Hao, M., Freymueller, J., Wang, Q. et al. (2016). Vertical crustal movement around the southeastern Tibetan Plateau constrained by GPS and GRACE data. *Earth Planet. Sci. Lett.*, 437, 1–8. DOI: 10.1016/J.EPSL.2015.12.038.

Kusche, J., Schmidt, R., Petrovic, S. et al. (2009). Decorrelated GRACE time-variable gravity solutions by GFZ, and their validation using a hydrological model. *J. Geod.*, 83, 903–913. DOI: /10.1007/s00190-009-0308-3.

Lenczuk, A., Leszczuk, G., Klos, A. et al. (2020). Study on the inter-annual hydrology-induced deformations in Europe using GRACE and hydrological models. *J. Appl. Geod.*, 14(4), 393–403. DOI: 10.1515/jag-2020-0017.

Liu, R., Li, J., Fok, H. et al. (2014). Earth surface deformation in the north China plain detected by joint analysis of GRACE and GPS data. *Sensors*, 14(10), 19861–19876. DOI: 10.3390/s141019861.

Loomis, B.D., Rachlin, K.E., and Luthcke, S.B. (2019a). Improved Earth oblateness rate reveals increased ice sheet losses and mass-driven sea level rise. *Geophys. Res. Lett*, 46, 6910–6917. DOI: 10.1029/2019gl082929.

Loomis, B.D., Luthcke, S.B., and Sabaka, T.J. (2019b). Regularization and error characterization of GRACE mascons. *J. Geod.*, 93, 1381–1398. DOI: 10.1007/s00190-019-01252-y.

Loomis, B.D., Rachlin, K.E., Wiese, D.N. et al. (2020). Replacing GRACE/GRACE-FO with satellite laser ranging: Impacts on Antarctic Ice Sheet mass change. *Geophys. Res. Lett*, 47(3), e2019GL085488. DOI: 10.1029/2019GL085488.

Peltier, W.R., Argus, D.F., and Drummond, R. (2015). Space geodesy constrains ice age terminal deglaciation: The global ICE-6G_C (VM5a) model. *J. Geophys. Res. Solid Earth*, 120(1), 450–487. DOI: 10.1002/2014JB011176.

Ries, J., Bettadpur, S., Eanes, R. et al. (2016). The Combined Gravity Model GGM05C. GFZ Data Services. DOI: 10.5880/icgem.2016.002.

Sun, Y., Riva, R., and Ditmar, P. (2016). Optimizing estimates of annual variations and trends in geocenter motion and J2 from a combination of GRACE data and geophysical models. *J. Geophys. Res. Solid Earth*, 121(11), 8352–8370. DOI: 10.1002/2016JB013073.

Tan, W., Dong, D., Chen, J. et al. (2016). Analysis of systematic differences from GPS-measured and GRACE-modeled deformation in Central Valley, California. *Adv. Space Res.*, 57(1), 19–29. DOI: 10.1016/j.asr.2015.08.034.

Tangdamrongsub, N., and Šprlák, M. (2021). The assessment of hydrologic-and flood-induced land deformation in data-sparse regions using GRACE/GRACE-FO data assimilation. *Remote Sens.*, 13(2). DOI: 10.3390/rs13020235.

Tesmer, V., Steigenberger, P., Dam, T. et al. (2011). Vertical deformations from homogeneously processed GRACE and global GPS long-term series. *J. Geod.*, 85, 291–310. DOI: 10.1007/S00190-010-0437-8.

Tregoning, P., Watson, C., Ramillien, G. et al. (2009). Detecting hydrologic deformation using GRACE and GPS. *Geophys. Res. Lett*, 36(15). DOI: 10.1029/2009GL038718.

van Dam, T., Wahr, J., and Lavallée, D. (2007). A comparison of annual vertical crustal displacements from GPS and Gravity Recovery and Climate Experiment (GRACE) over Europe. *J. Geophys. Res. Solid Earth*, 112(B3). DOI: 10.1029/2006JB004335.

Wahr, J., Molenaar, M., and Bryan, F. (1998). Time variability of the Earth's gravity field: Hydrological and oceanic effects and their possible detection using GRACE. *J. Geophys. Res. Solid Earth*, 103(B12), 30205–30229. DOI: 10.1029/98JB02844.

Wahr, J. (2007). Time-variable gravity from satellites. *Treatise on geophysics*, 3, 213–237. DOI: 10.1016/B978-044452748-6.00176-0.

Wang, L., Chen, C., Ma, X. et al. (2020). Evaluation of GRACE mascon solutions using in-situ geodetic data: The case of hydrologic-induced crust displacement in the Yangtze River Basin. *Sci. Total Environ.*, 707, 135606. DOI: 10.1016/j.scitotenv.2019.135606.

Wang, P., Wang, S.Y., Li, J. et al. (2023). Comparison of GRACE/GRACE-FO Spherical Harmonic and Mascon Products in Interpreting GNSS Vertical Loading Deformations over the Amazon Basin. *Remote Sens.*, 15(1), 252. DOI: 10.3390/rs15010252.

Yin, G., Forman, B.A., Loomis, B.D. et al. (2020). Comparison of vertical surface deformation estimates derived from space-based gravimetry, ground-based GPS, and model-based hydrologic loading over snow-dominated watersheds in the United States. *J. Geophys. Res. Solid Earth*, 125(8), e2020JB019432. DOI: 10.1029/2020JB019432.